Research article

Mohammed Lamine Mekhalfia*

Optimization of thermal energy harvesting by PZT using shape memory alloy

https://doi.org/10.1515/ehs-2020-0003
Received November 26, 2020; accepted February 28, 2021; published online March 23, 2021

Abstract: Thermal Energy harvesting intends to supply portable or wireline electrical appliances connected to a generator with the necessary power on the purpose of making them energy-independent. The implemented power values in this case are small; they range from Microwatt to Watt. This self-feeding process is an attempt to cope with the widespread energy-efficient electronic technologies of nowadays. Additionally, this study aims at recovering renewable micro-energy by means of the piezoelectric material and optimizing its efficiency by using Shape Memory Alloys (SMAs). This study sheds light upon the progress made on storage devices that are necessary to compensate for the intermittencies and the inadequacies that occur in the production and consumption of the generated electrical energy.

Keywords: energy management; piezoelectricity (PZT); shape memory alloy (SMA); thermal energy harvesting.

Introduction

When a very large number of sensors scattered in a harsh environment, a need for a power supply to limit maintenance urges and this would be impossible in some circumstances like confined spaces, heat, lack of air, or toxic chemical. What solutions to come up with to make use of a source of infinite energy provided in the immediate environment of the sensor?

Thermal energy is the considered source; present in many environments and likely to provide enough energy to empower a sensor (Lobontiu 2007; Stoyanov 2011; Tchawou 2014).The objective is to develop an energy harvester which converts this available energy as efficiently as possible and in the smallest possible volume.

Piezoelectricity (PZT) is the property of some materials to generate electricity under the action of a constraint and to deform under the application of an electric field. A piezoelectric micro-generator behaves as an oscillating weight attached to a beam. When the mass oscillates, the stresses in the beam generate a voltage in the piezoelectric layer. We manage these millivolts at the exit of this type of structure. The function of the associated electronics is to straighten the low alternating voltages from the micro-generator and to raise it so that it can be useful (Bathias 2013; Brunet 2009). If yields are sufficient, it is possible to use them to supply different types of sensors: Temperature, pressure, vibration, humidity, brightness, air quality …

There are two types of micro piezoelectric generators: Micro-generators operating in quasi-static mode which are excited at much weaker frequencies as their resonant frequency, and micro-generators running in dynamic mode that are excited at frequencies approximate to their resonant frequency (Papet 2012).

To present the coupling between piezoelectric element and Shape Memory Alloy (SMA) materials, a description to SMA phenomenon is inevitable. SMA are materials with the ability to change shape. When cooling down, the SMA undergoes two transitions called Martensitic and Austenite (Hot state) transformations, respectively. Direct and reverse transformation occurs within a defined temperature interval from the start to the end where 'A_s' refers to the start whereas 'A_f' stands for the end point of this interval. A large stress and strain produced during such a change depends on the type of the used alloys: Wide temperature intervals correspond to a large strain and stress, and the choice of the optimal alloy depends on the objective of applications. An adjustment of characterization is also required for energy harvesting because of the significant dependence of SMA characteristics with surrounding environment.

The conversion of mechanical to electrical energy must be optimal in order to achieve a maximum power. This work is interested in electromechanical energy conversion

*Corresponding author: Mohammed Lamine Mekhalfia, Department D 3 Dynamics and Vibration, Institute of Thermomechanics, Czech Academy of Sciences, Prague, Czech Republic,
E-mail: mohammedlaminemekhalfia@gmail.com. https://orcid.org/0000-0002-3653-3517

and on the harvesting circuit that permits the conversion of the produced voltages into useful ones that can empower the charge (Leo 2007).

In this research paper, a standardized theoretical model of a piezoelectric generator is to be presented, allowing the study of the effect that temperature has on it. Then the combination of SMAs those are also adapted to the change in thermal energy and transformed in a more efficient way into mechanical energy. Then study of added value of their effect on Piezoelectric/SMA combination system. A set up of power management circuit used to ensure operation mode with optimal parameters of the energy system to achieve best conversion factors and the highest efficiency.

Piezoelectric system

Going back to the quasi-static piezoelectric system that is defined by its excitation frequencies, these must be weaker than the system's resonant frequency.

The effect of PZT is distinguished by two mode of function, the first is called the direct mode and the second is the reverse or "the Indirect" mode. The direct mode is the phenomenon that describes the appearance of an electric field when the material is under a mechanical force. The inverse is defined by a mechanical distortion of the PZT material under the effect of an electrical field (Ahmed-Seddik 2012).

Description of PZT system

Generally, the piezoelectric Element used in mode 33, where tension and stress act in direction 3, can also work with mode 31. In this case, tension acts following direction 3, stress and deformation work on direction 1. Operation in mode 31 involves the use of elements for which a significant deformation is generated by bending towards direction 1 (see Figure 1).

Thirty one elements are bi-morphs with two connected piezoelectric layers sets and are the most common type used.

During bending, the upper surface is in tension while the lower is in compression or vice versa. Therefore, each layer is polarized in the same way. Similarly, with the electrodes correctly connected, the currents produced are added (parallel polarization). If the layers are reversely polarized, the voltages are added (serial polarization); in both cases, the conversion potential remains constant. In theory, the polarization and the number of layers act only on the ratio between the voltage and the current. We consider a cantilever structure. This structure has a lower stiffness for a given size. Then, for some input strength, it generates the greatest constraint.

Electromechanical analogy

This analogy verifies the classical conversion between electrical and mechanical quantities (Table 1). Thus, a system {mass, spring, damper} can be modelled by an impedance RLC, usually referred to as the emotional branch (Figure 2).

Table 1: Conversion of mechanical to electrical quantities (Boisseau 2011).

Mechanical quantities	Electrical quantities
Displacement: u (m)	Electrical charge: Q (C)
Speed: V (m/s)	Courant: I (A)
Force: F (N)	Voltage: U (V)
Mass: m (kg)	Inductance: L (H)
Stiffness: k (N/m)	Capacity: C (F)
Depreciation: ρm (kg/s)	Resistance: R (Ω)
Recessed end: $V = 0$	$I = 0$
Free end: $F = 0$	$U = 0$

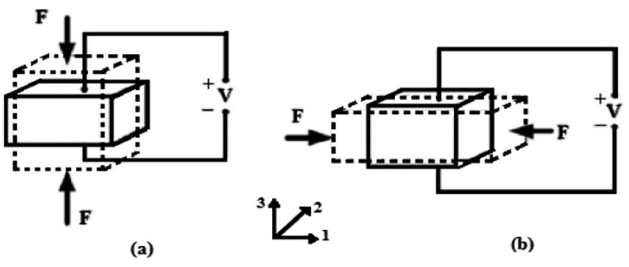

Figure 1: PZT working mode.
(a) mode 33 (b) mode 31 (Ahmed-Seddik 2012).

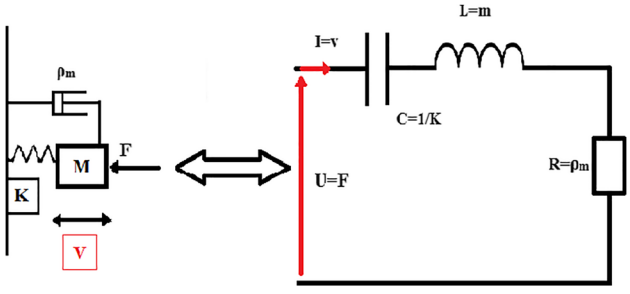

Figure 2: Equivalence between mechanical and electrical system (Boisseau 2011).

Equivalent circuit in quasi-static mode

The generator implemented in this work is intended to recover the energy where the frequency of mechanical stress applied on the piezoelectric device is very low compared to its resonance mode. The quasi-static model is therefore solely determined from static equations of PZT. It is possible to obtain this model from the dynamic models, by simply tilting the frequency to zero. In this case, the inductive elements as well as mechanical losses will not be taken into account since their values may be ignored at low frequencies

Long piezoelectric bar deformed according to mode 33

Considering a parallelepiped PZT bar polarized according to the height mentioned in Figure 4, we assume that it is subjected to a uniform force F applied over its entire surface and that it is deformed according to mode 33 (a constraint along the axis of polarization causes deformation along the same axis) (see Figure 3). Other modes of mechanical deformation are assumed to be negligible and the height of the bar being big in front of the transverse dimensions; additionally, only the component along axis 3 is to be considered for all the studied quantities; also, losses not taken into account in this part.

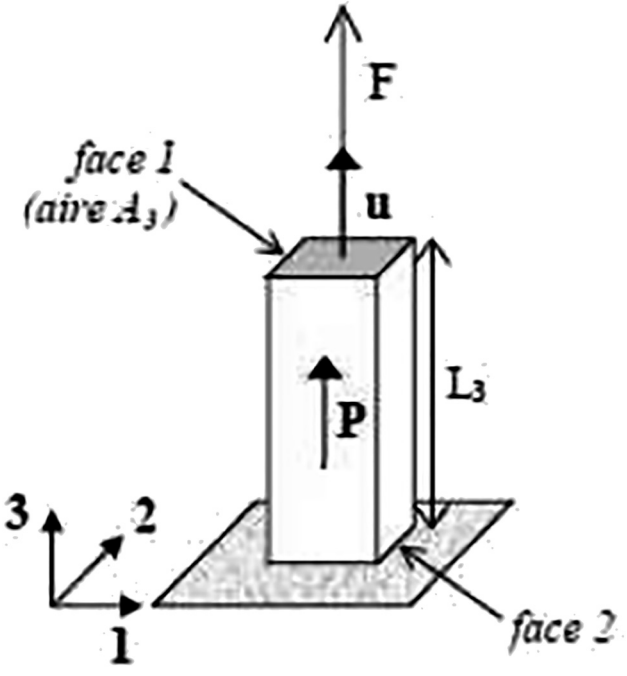

Figure 3: PZT bars in mode 33 (Defosseux 2011).

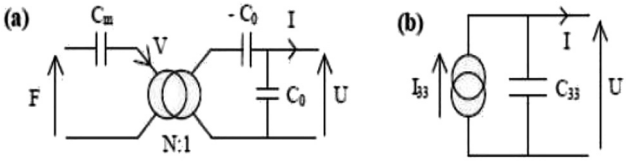

Figure 4: Equivalent circuit to PZT bars in mode 33 (Defosseux 2011).

The ratings are as follows:

- L_3: height of the bar;
- A_3: area of the section of the bar;
- P: dielectric polarization; V: speed of the end of the bar;
- F: force applied to the end of the bar;
- u: displacement of the end of the bar;
- U: tension between the two ends of the bar;
- I: current through the bar;
- T_3: stress;
- S_3: relative deformation;
- E_3: electric field;
- D_3: electrical induction.

These quantities linked by:

$$T_3 = \frac{F}{A_3}\ S_3 = \frac{u}{L_3}\ E_3 = -\frac{U}{L_3} \quad I = A_3\ \frac{dD_3}{dt} \tag{1}$$

In addition, electromechanical coefficients are:

β_{33}^S et β_{33}^T Inverse of the dielectric permittivity at S or T constant;

S_{33}^D Elastic flexibility at constant D;

g_{33}eth_{33} Piezoelectric coefficients.

Equivalent circuits take into account the propagation of the mechanical wave in the piezoelectric material. In the case of the generator presented here, the presented model is therefore determined solely from the static equations of PZT. The equations chosen to establish the equivalent model are:

$$S_3 = S_{33}^D T_3 + g_{33} D_3 \tag{2}$$

$$E_3 = -g_{33} T_3 + \beta_{33}^T D_3 \tag{3}$$

We deduce that

$$E_3 = -h_{33} S_3 + \beta_{33}^S D_3 \tag{4}$$

$$\left(1 - \frac{g_{33} h_{33}}{\beta_{33}^S}\right) S_3 = S_{33}^D T_3 + \frac{g_{33}}{\beta_{33}^S}\ E_3 \tag{5}$$

$$\left(\frac{\beta_{33}^S}{g_{33}} - h_{33}\right) u = \frac{S_{33}^D}{g_{33}}\ \frac{\beta_{33}^S L_3}{A_3}\ F - U \tag{6}$$

where C_0 is built-in ceramic capacity

$$C_0 = \frac{A_3}{\beta_{33}^S L_3} N = h_{33} C_0 \tag{7}$$

$$\left(\frac{\beta_{33}^S}{h_{33} C_0 g_{33}} - \frac{1}{C_0} \right) Nu = \frac{1}{N} F - U \tag{8}$$

where C_m is the mechanical capacity in Law frequency mode.

$$C_m = \frac{S_{33}^D L_3}{A_3} \tag{9}$$

$$\left(\frac{1}{N^2 C_m} - \frac{1}{C_0} \right) NV = \frac{d}{dt} \left(\frac{1}{N} F - U \right) \tag{10}$$

$$-\frac{1}{L_3} \frac{dU}{dt} = -\frac{h_{33}}{L_3} \frac{du}{dt} + \frac{\beta_{33}^S}{A_3} I \tag{11}$$

$$C_0 \frac{dU}{dt} = NV - I \tag{12}$$

$$\begin{cases} \left(\frac{1}{N^2 C_m} - \frac{1}{C_0} \right) NV = \frac{d}{dt} \left(\frac{1}{N} F - U \right) \\ NV - I = C_0 \frac{dU}{dt} \end{cases} \tag{13}$$

Equation (13) reveals the electromechanical analogy between voltage and force current – speed. The coefficient N, with F as its weight force and V as its speed, suggests the introduction of a transformer N:1 ratio; thus connecting the two mechanical and electrical branches. This transformer, associated with the negative capacitance $-C_0$, models the electromechanical conversion due to PZT.

This circuit can be in the form of an equivalent Norton generator, including I_{33} current source and Z_{33} parallel impedance:

$$\begin{cases} I_{33} = \frac{F}{N} \frac{1}{\frac{1}{j\omega N^2 C_m} - \frac{1}{j\omega C_0}} \\ Z_{33} = \frac{N^2 C_m}{C_0} \left(\frac{1}{j\omega N^2 C_m} - \frac{1}{j\omega c_0} \right) \end{cases} \tag{14}$$

In the time domain, the piezoelectric bar is equivalent to a current source proportional to the derivative of the applied force, in parallel with a capacitance C_{33} (Figure 4b):

$$\begin{cases} I_{33}(t) = A_{33} \frac{dF}{dt}, \quad A_{33} = \frac{N C_m C_0}{C_0 - N^2 C_m} \quad \left(\frac{C}{N} \right) \\ C_{33} = \frac{C_0^2}{C_0 - N^2 C_m} \end{cases} \tag{15}$$

Characteristics of the piezoelectric P188

The used PZT is a cylinder with a radius of 2 cm and thickness of 0.33 mm, constituted by PZT ceramic of P188 of Quartz and Silicon.

Table 2 shows the characteristics of the materials and the parameters of the model. The frequency of the applied force is much less weaker than the natural frequency of the system vibration.

System feedback for exponential constraint

Considering the previous bars connected in parallel to RC charge.

Supposed that the mean value of Force $F(t)$ applied on the bar section has an exponential form:

$$F(t) = F_0 \left[1 - \exp\left(-t/\tau_m \right) \right] \tag{16}$$

Source of courant I_{33}:

$$I_{33}(t) = \frac{A_{33}}{\tau_m} F_0 \exp\left(-t/\tau_m \right) \tag{17}$$

The differential equation becomes:

$$R I_{33}(t) = \tau \frac{dU}{dt} + U \quad ou \, \tau = R(C + C_{33}) \tag{18}$$

The solution of this equation is under the form:

$$\begin{cases} U(t) = (U_i + U_p) + \exp(-t/\tau) - U_p \exp(-\tau/\tau_m) \\ U_i = U(0) \\ U_p = \frac{A_{33} F_0 R}{\tau - \tau_m} \end{cases} \tag{19}$$

Table 2: PZT characteristics and model parameters (Defosseux 2011).

Characteristics of PZT P188	Model parameters
$S_{33}^D = 9.09.10^{-12}$ m²/N	$A_{33} = 4.25.10^{-10}$
$\epsilon_{33}^T = 1850\ \epsilon_0$	$C_{33} = 14.7$ pF
$g_{33} = 26.10^{-3}$ Vm/N	$C_0 = 6.64$ pF
$\tan\delta \leq 0.02$	$C_m = 10{,}1$ nF
$Q_m = 80$	$N = 19{,}0.10^{-3}$

Relation between temperature and mechanical force

Relation of the perfect gas:

$$P \times V = n \times R \times \theta \tag{20}$$

P: Pressure in Pa.
V: Volume.
n: Number of moles.
R: 8.31 J mol^{-1} K^{-1}.
θ: Temperature in kelvin.

Therefore, if we enclose a certain amount of gas in a constant envelope volume V, the pressure developed by the gas is proportional to the absolute temperature:

$P = RT/V$ with R/V constant.

Pressure will be calculate as force by surface

$$P = F/s \tag{21}$$

Results

Under a temperature gradient ΔT = 40 °C which can give us/yield a force F = 0.001 N according to the volume and the surface of the used PZT. Obtained from the simulation, responses related to voltage and as function of resistance R is shown in Figure 5.

The resulted curve represents the voltage variation as a function of the resistance and where the PZT is modelled by a current source; the voltage path follows the path required by the RC load. We can distinguish two zones: The transient zone where the linear variation demonstrates a fast response of the voltage and the second indicates the steady state of the operation after a resistance of 1.5 10^5 Ω.

Observing the curves representing the instantaneous power applied during the compression cycle of the PZT (Figure 6), we noticed that the area under each curve corresponds to the energy supplied or received over the considered interval.

During compression, the PZT supplies the mechanical energy from which a large part is stored in an elastic form by the compressed PZT, the rest of it supplied to the resistive load, the energy supplied to the internal capacitor C_0 is zero.

In the second phase, the mechanically stored energy supplies the source because the speed on the surface of the bar is negative while the applied force decreases in being positive. This highlights the importance of the applied stress form: It should be zero while the bar relaxes, in order to provide the electric charge with all the mechanical energy stored by the PZT.

Considering that the losses would not change the obtained results, it is worth mentioning that they are of three natures: mechanical, dielectric and piezoelectric; and that they depend on the frequency and intensity of the electric field.

Precise modelling goes beyond the scope of this study, especially since they were neglected in the case of quasi-static operations.

Shape memory alloy

SMAs? are becoming day after day better known and much more used. A plethora of applications have emerged within the last couple of years in different fields such as Biomedical and Aerospatiale, and Robotics. SMAs are deployed thanks to their form memory, super-elastic, or damping effect proprieties.

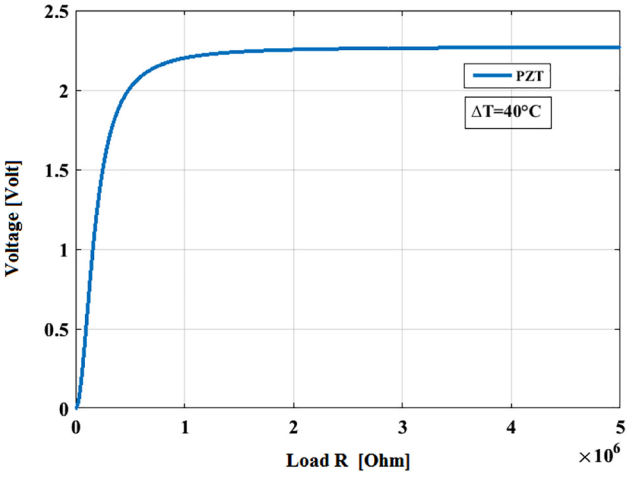

Figure 5: Voltage variation accroding to load R.

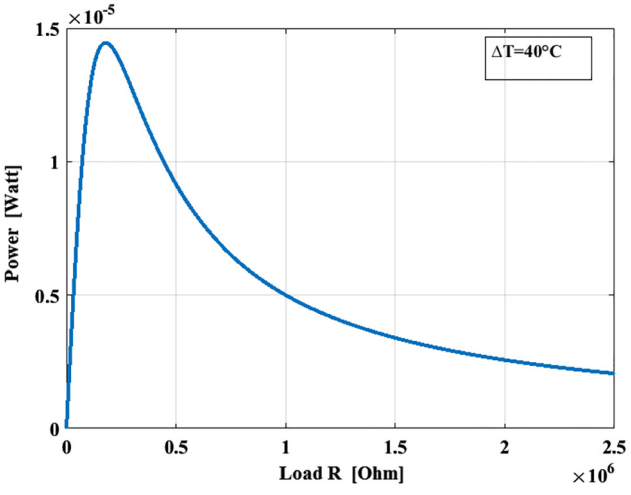

Figure 6: PZT power variation according to load R.

Nickel Titanium, also known as Nutinol is a metal alloy made up of Nickel and Titanium; this name is derived from Nickel Titanium-Naval Ordnance Laboratory. William J. Buehler (Buehler, Gilfrich, and Wiley 1963) along with Frederick Wang (Wang, Buehler, and Pickart 1965), discovered its properties while conducting a research at the Naval Ordnance Laboratory in the year 1959 (Kauffman and Mayo 1997; The Alloy That Remembers 1968).

Mono dimensional model

The comportment of SMA modulation, which is based on the Martensitic variant's phase transition, is a temperature-managed process. Müller, Achenbach, and Seelecke demonstrate that the potential energy of Martensitic variables is given by the free energy of Gibbs or, in the absence of solicitation, by the Free energy of Helmholtz (Smith 2005). By considering an uni-axial load, assumed to coincide with x1 direction, the model of SMAs is then reduced to 1D model. The stress tensor has only one non-zero component that is:

$$\sigma_{11} = \sigma \neq 0 \tag{22}$$

The transformation strain components given by

$$\epsilon_{11}^t = \epsilon^t \; ; \epsilon_{22}^t = \epsilon_{33}^t = -\frac{1}{2}\,\epsilon^t \; ; \epsilon_{12} = \epsilon_{23} = \epsilon_{31} = 0 \tag{23}$$

ϵ^t is the axial transformation strain, assuming that its results in isochoric deformations occur due to phase transformation.

The demonstration replaced by the following equations to summarize the 1D thermo-mechanical model (Lagoudas 2008).

Thermo-elastic response:

$$\epsilon = S^A\sigma + \alpha^A\,(T - T_0) \quad \text{or}\, \epsilon = S^M\sigma + \alpha^M\,(T - T_0) \tag{24}$$

Forward phase transformation:

$$\pi = |\sigma|H + \frac{1}{2}\,S\sigma^2 + \rho s_0 T - \rho u_0 - \left[\begin{array}{l} \rho b^M \xi + \\ (\mu_1 + \mu_2) \end{array}\right] = Y \tag{25}$$

$$\epsilon = S\sigma + \alpha\,(T - T_0) + \frac{Hsgn(\sigma)}{\rho b^M}\left[\begin{array}{l} |\sigma|H + \\ \frac{1}{2}\,S\sigma^2 + \\ \rho S_0\,(T - M_s) \end{array}\right] \tag{26}$$

Reverse phase transformation:

$$\pi = |\sigma|H + \frac{1}{2}\,S\sigma^2 + \rho s_0 T - \rho u_0 - \left[\begin{array}{l} \rho b^A \xi + \\ (\mu_1 + \mu_2) \end{array}\right] = -Y \tag{27}$$

$$\epsilon = S\sigma + \alpha\,(T - T_0) + \frac{Hsgn(\sigma)}{\rho b^A}\left[\begin{array}{l} |\sigma|H + \\ \frac{1}{2}\,S\sigma^2 + \\ \rho S_0\,(T - A_f) \end{array}\right] \tag{28}$$

Parameters

See Table 3.

Table 3: Ni-ti SMA model parameters (Qi 2011).

Density (g.cm^{-3})	**6.4–6.5**
Young module in traction *E* (GPa)	70–98 (A)/20–35 (M)
Austenite yield strength (MPa)	100–800
Martensitic yield strength (MPa)	50–300
Break load (MPa)	800–1500
Transformation temperatures (°C)	−200 a + 120
Transformation enthalpy (J.g^{-1})	19–28
Transformation hysteresis (°C)	20–40
Maximum recoverable tensile strain by memory (%) (mono-crystal)	6–8
Super-elastic strain (%)/mono-crystal	10
Super elastic strain (%)/polycrystal	4–10
Melting temperature (°C)	1240–1310
Thermal conductivity (W/m.K)	18 (A)/8.6 (M)
Coefficient of thermal expansion (10ˆ−6/K)	10–11 (A)/6.6 (M)

Results

Variations in the external temperature ignite the Memory Form effect, an effect followed by the phenomenon of super elasticity. A gradient of a 40 °C shows a reversible deformation of a 4% max. The applied effort helps to produce a force cycle that can reach 300 MPA where the force doesn't return to its initial state "0 MPa" because the transformation A-M, M-A does not form a closed cycle 'total inverse transformation' (see Figure 7).

Thermal energy harvesting by piezoelectric element with shape memory alloy

PZT materials have the possibility to transform the mechanical energy to an electric in order to secure power supply to a greater number of equipments. This work is based on amplifying the temperature effect over PZT to

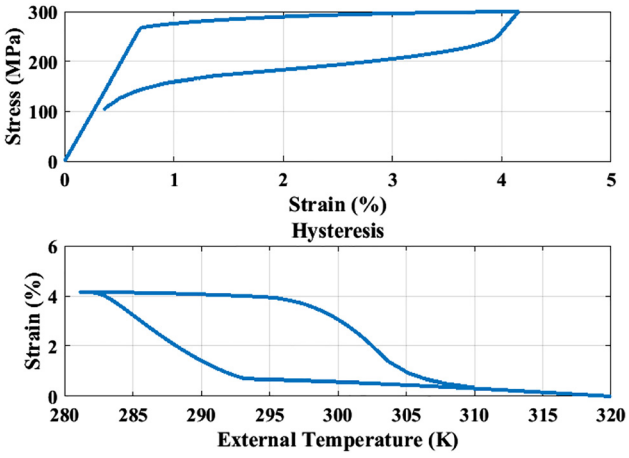

Figure 7: Up) Relation stress strain – Down) Strain variation according to external temperature.

enhance the energy conversion and to maximize the produced electrical energy (Jordan and Rocher 2009–2010).

The SMA-PZT element is under study, the study of thermo-mechanical and Mechanic-electrical interactions, the force generated from the SMA considered as PZT constraint (Lexcellent 2013).

A prototype is set and simulated using MATLAB to module the harvested energy under a 40 °C gradient, a frequency of 0.5 Hz and a conservation to previous parameters mentioned in the study in AMF and PZT.

The thermo-electrical generator used to produce thermal effect, a reverse switch between hot/cold sides on both generators will create the needed gradient and the abetment of form memory effect of SMA (see Figures 8–11).

Power and voltage figures according to load *R* show the important evolution upon SMA use, the SMA play the role of a force (power) amplifier.

SMA can generate a 0.0037 N higher than the force generated by the temperature gradient, in the same condition we obtain a max power of 10 times higher using SMA, the voltage develops from 2.2 to 9.2 V (see Figure 12).

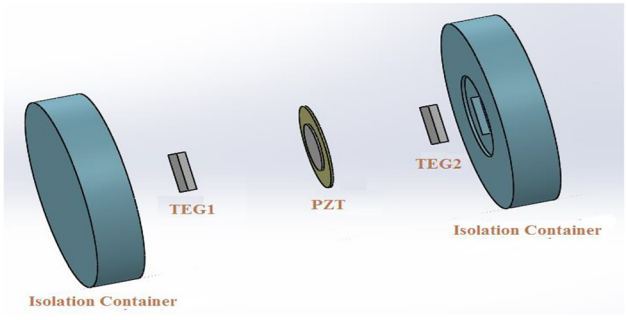

Figure 8: Prototype thermal energy harvesting using PZT.

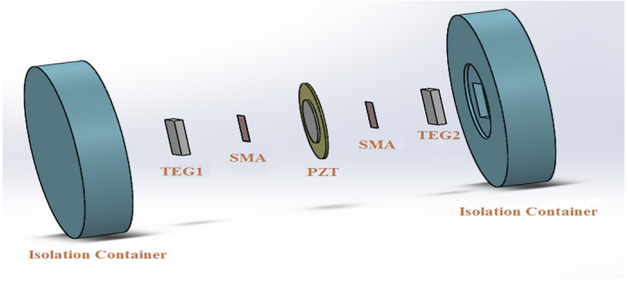

Figure 9: Prototype thermal energy harvesting using SMA-PZT.

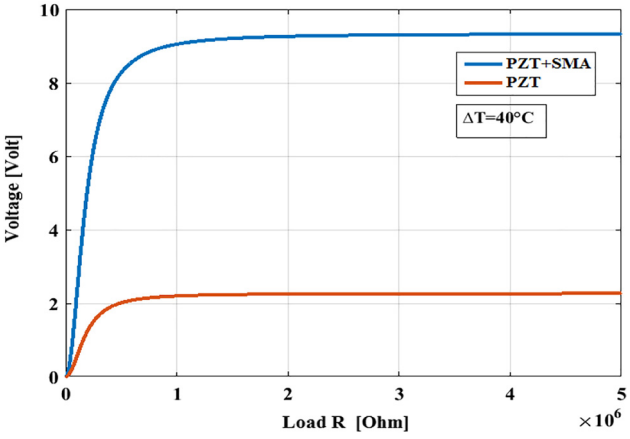

Figure 10: PZT voltage variation according to load *R* (with/without SMA).

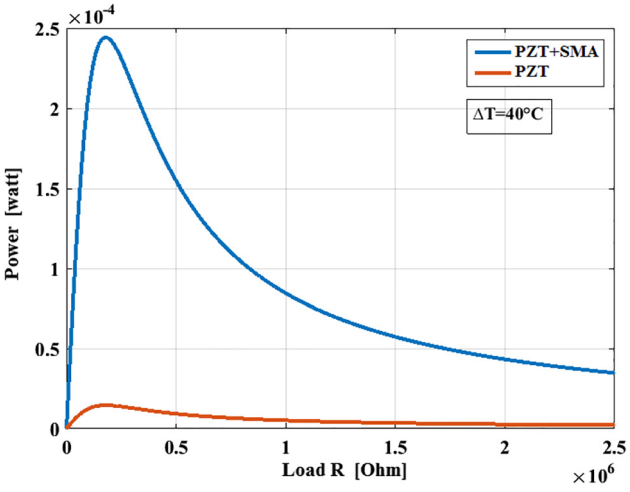

Figure 11: PZT power variation according to load *R* (With/without SMA).

We notice a huge dependence between the power, frequency and resistance. The variation is almost linear, shows a continuous increase in power according to frequency. In the same time the power curve characterized by two phases: The first 1st is an energy transfer to storage and

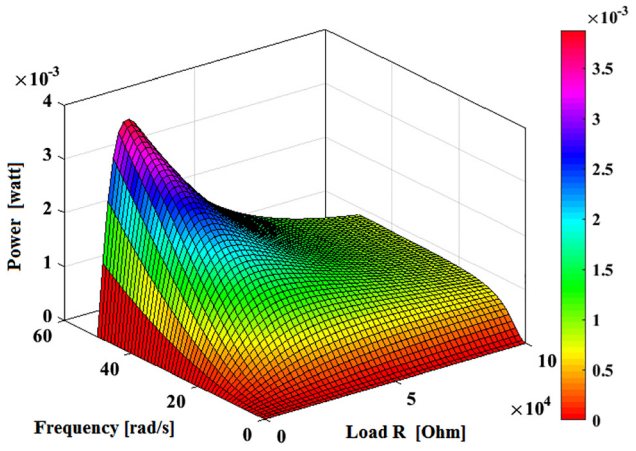

Figure 12: 3D view of PZT + SMA power variation in function of load *R* and frequency *F*.

charge, the second 2nd represents a dissipation of the total stored energy to the Load because the stress applied is null.

The maximum power point corresponds to the optimal load; *R* (resistance) varies also in function to the frequency and represents a translation point from the 1st Phase to the 2nd.

Energy management

This circuit aims to rectify the alternating voltage V_p of the piezoelectric generator with the AC/DC converter, and then supply the energy harvested to the battery through the DC/DC voltage adaptation circuit.

When partitioning the autonomous micro-system, the energy management circuit is the subsystem constituting the analog/digital electronic part. This circuit consists of linear (resistors, capacitors, inductance) and non-linear (diodes, MOSFETs) electrical elements and a digital control part.

The models developed using MATLAB and particularly the technique of programming for power electronics circuits, which we adapt for our application.

We previously mentioned that the AC voltage produced by the generator must be adapted to empower the battery. The main function of the power management circuit is to condition the generator signal, and transform it into a DC current to charge the storage element.

The energy management circuit performs two tasks:

- The conversion of the AC signal at the output of the piezoelectric generator into a continuous signal by rectification with an AC/DC converter.
- The adaptation of the voltage supplied by the AC/DC for a specific battery by transfer of maximum power. This function performed by a DC/DC converter is composed by the compensator, command and controller circuits.

The block diagram of the energy management circuit is given in Figure 17 (box block). The alternating voltage of the piezoelectric generator V_p is rectified into a DC voltage V_{rect}, which in turn is adapted to obtain the voltage across the battery V_{bat}. In this case, the power management circuit acts as a power source for the battery (see Figure 13).

AC/DC rectifier

The full-wave AC/DC rectifier consists of a Graëtz bridge and a C_{rect} capacitor (Figure 15). In order that Graëtz bridge diodes conduct, it is necessary that the voltage delivered by the transducer V_p be greater than diode's threshold voltage. This problem does not arise when we use large generator dimensions that provide higher voltages and higher powers than losses introduced by the diodes (see Figure 14).

The current of the piezoelectric generator i_p is a sinusoidal signal. As long as the voltage at the terminals of C_{piezo} is lower than the voltage V_{rect}, the diodes remain blocked and the output current i_o (t) is zero. When this voltage becomes higher, the current flows to the capacity C_{rect} and loads.

The current i_o (t) can be described as follows:

$$i_0(t) = 0 \qquad 0 < \omega t < u \tag{29}$$

$$i_0(t) = \frac{C_{\text{rect}}}{C_{\text{rect}} + C_p} I_p |\sin(\omega t)| \qquad u < \omega t < T \tag{30}$$

In our case, we assume that the capacity C_{rect} is much larger than the capacity C_{piezo} which allows a good filtering of the AC voltage and that the voltage V_{rect} is considered constant. The expressions of the average current $i_o(t)$ as a function of the generator current amplitude I_p and of the output voltage V_{rect} as well as the average power recovered P_{average} are given by:

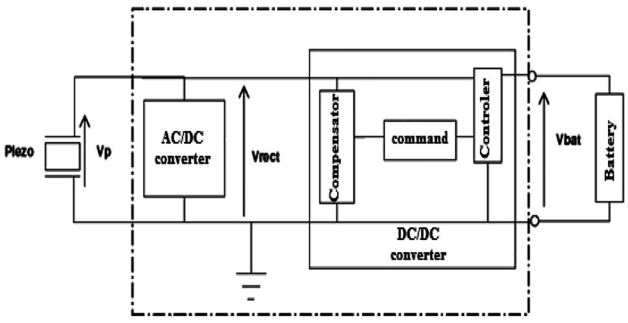

Figure 13: Schematic bloc of energy management circuit (Zenati 2007).

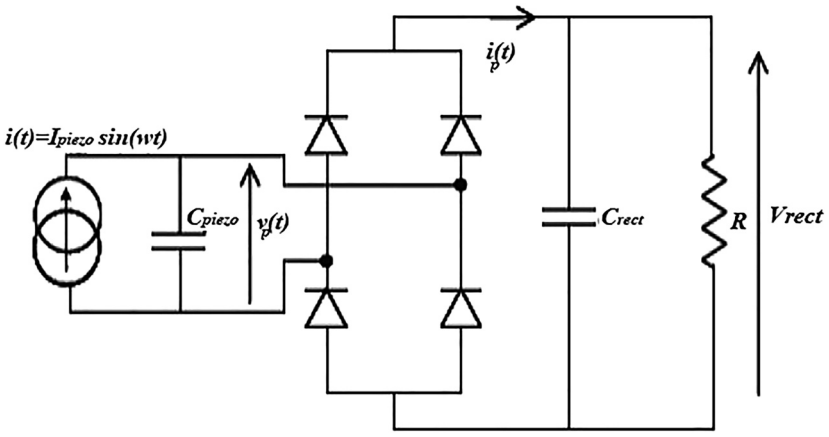

Figure 14: Electric schematic of AC/DC converter (Zenati 2007).

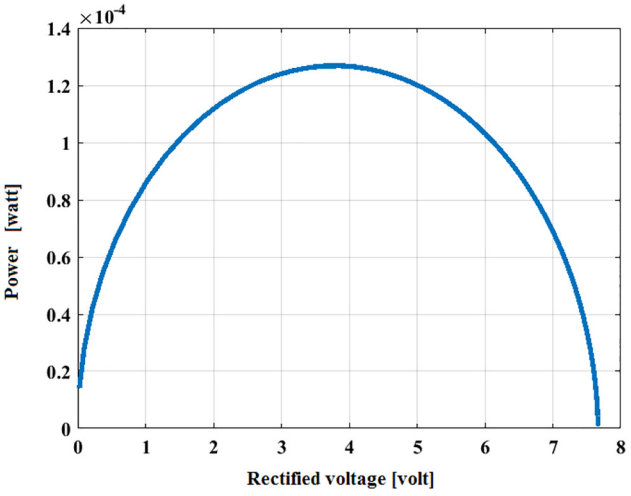

Figure 15: Power in function of rectified volatge.

$$i_0(t) = \frac{2I_p}{\pi} - \frac{2V_{\text{rect}}\omega C_{\text{piezo}}}{\pi} \tag{31}$$

$$P_{\text{average}} = \frac{2V_{\text{rect}}}{\pi}\left(I_p - V_{\text{rect}}\omega C_{\text{piezo}}\right) \tag{32}$$

$$V_{\text{rect}} = \frac{I_p}{2\omega C_{\text{piezo}}} \tag{33}$$

The figure above gives the value of the power after conversion, It is clearly seen that the power depends on the voltage V_{oc} (rectified output voltage); the maximum power reached for an optimum voltage is equal to half of the no-load voltage.

DC/DC converter

In our case, we assume that the piezoelectric transducer delivers a higher voltage than the battery. To adapt the input voltage V_{rect} to the battery voltage V_{bat}, we used a voltage step-down, this circuit is represented by Figure 16. Allow also avoiding current passage into AC/DC converter. In steady state, the voltage across the battery is almost constant, and therefore the transfer of maximum power is done by electric current.

Two operating modes exist in step-down converter function: continuous and discontinuous mode. The discontinuous mode corresponds to the cancellation of the current in the inductance during a period of operation. This situation occurs when the average current absorbed by the load is less than half of the current ripple in the inductor. The continuous mode of operation has as characteristics a less corrugated current output, lower constraints on the devices, but a reaction time longer than the discontinuous mode. In both modes, the converter is characterized by a discontinuous input current which implies a harmonic disturbance in the power source.

The discontinuous mode of operation is interesting for applications that require a certain feedback speed to the variation of the load and/or the input voltage. Contrariwise, this mode causes a large current in inductor, and a high capacity for output filtering (Qi 2011). The transfer function of the converter operating in discontinuous mode is:

$$\frac{V_s}{V_e} = \frac{\alpha}{\alpha + \grave{\alpha}} \tag{34}$$

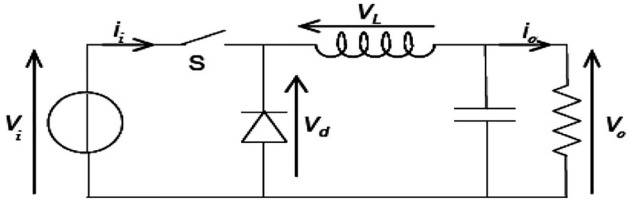

Figure 16: BUCK converter schematic (Zenati 2007).

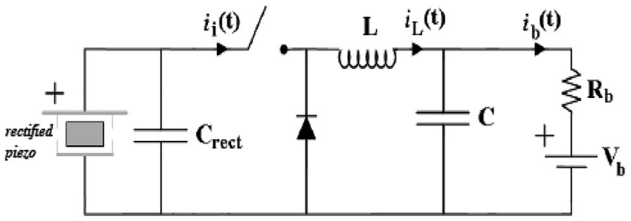

Figure 17: Studied model to cyclic ration calculation (Zenati 2007).

Inductor current determined by the following expressions:

$$i_L(t) = \frac{V_e - V_s}{L} t \quad 0 < t < \alpha T \tag{35}$$

$$i_L(t) = I_M - \frac{V_s}{L}(t - \alpha T) \quad \alpha T < t < \dot{\alpha} T \tag{36}$$

$$i_L(t) = 0 \quad \alpha T < \dot{t} < T \tag{37}$$

$$I_M = \frac{V_e - V_s}{L} \alpha T = \frac{V_S}{L} \dot{\alpha} T. \tag{38}$$

The input current of the converter is

$$\langle i_e \rangle = \frac{\alpha}{2} I_M. \tag{39}$$

Output current

$$\langle i_L \rangle = \frac{I_M}{2}(\alpha + \dot{\alpha}) = \frac{\alpha^2}{2Lf_s} \frac{V_e}{V_s}(V_e - V_s). \tag{40}$$

Choice of L and C

$$L = \frac{V_i - V_o}{I_M f_s} \alpha \quad C = \frac{(I_M - i_0)^2 \alpha}{2 I_M f_s V_0} \frac{V_i}{V_o}. \tag{41}$$

So optimal cyclic ratio calculated from the model under (see Figure 18):

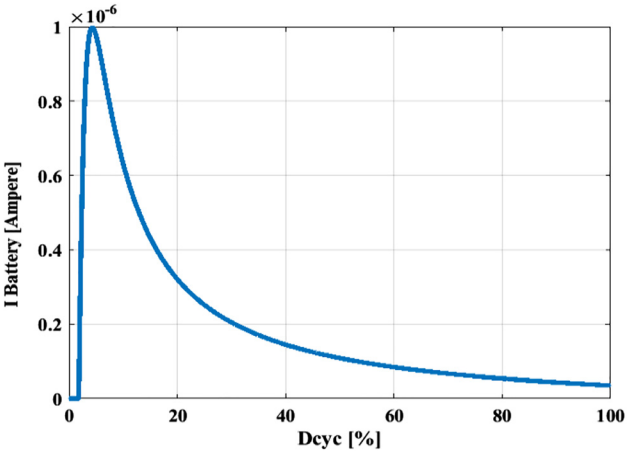

Figure 18: Battery courant variation in function of cyclic ratio.

$$\alpha = \sqrt{\frac{4Lf_S \omega C_p V_{\text{rect}}}{\pi (V_{\text{rect}} - V_b)}} \tag{42}$$

We report the current of the piezoelectric transducer curve according to the cyclic ratio, taking into account that the optimal duty cycle value for Ib equals $1*10^{-6}$ at 4.3% At this value, the Cyclic Duty Ratio is associated to the maximum value of the battery current for a $V_b = 4$ V.

Conclusion

This work consists of three main axes, the study of thermal piezoelectric reactions, the study and examination of Shape Memory Effect and their influence on thermal energy harvesting by PZT, and finally harvested energy management.

The simulation results made it possible to notice the advantage of using an associated mechanical system. The connection between PZT and AMF contributes to the improvement of the electromechanical conversion properties of PZT ceramics follows with thermal excitation. The structure proposed in this paper represents a good tool for estimating harvested energy and preferred candidates for ambient vibrations conversion into electricity to power the electrical systems.

Acknowledgment: An intensive and detailed study containing a wide explanation on model, characteristics and results may be found via the link Thermal Energy Harvesting.

Author contributions: The author has accepted responsibility for the entire content of this submitted manuscript and approved submission.

Research funding: None declared.

Conflict of interest statement: The author declares no conflicts of interest regarding this article.

References

Ahmed-Seddik, B. 2012. "Systèmes de récupération d'énergie vibratoire large bande." Thèse de Doctorat, L'Université de Grenoble.

Bathias, C. 2013. *Matériaux Composites*. Dunod: L'Usine Nouvelle.

Boisseau, S. 2011. "Récupération d'énergie vibratoire à électrets." Thèse de Doctorat, L'Université de Grenoble.

Brunet, Y. 2009. *Problématique du stockage d'énergie, France: Hermès – Lavoisier, Collection: Traité EGEM: Electronique – Génie Electrique – Microsystèmes*.

Buehler, W. J., J. W. Gilfrich, and R. C. Wiley. 1963. "Effects of Low-Temperature Phase Changes on the Mechanical Properties of Alloys Near Composition TiNi." *Journal of Applied Physics* 34 (5): 1475–7.

Defosseux, M. 2011. *Conception et caractérisation de microgénérateurs Piézoélectriques pour microsystèmes autonomes*. Grenoble, France: L'Université de Grenoble.

Jordan, L., and P. Rocher. 2009–2010. *Alliage à mémoire de forme, support de cours*. France: Société Francophone de Biomatériaux Dentaires.

Kauffman, G. B., and I. Mayo. 1997. "The Story of Nitinol: The Serendipitous Discovery of the Memory Metal and its Applications." *The Chemical Educator* 2 (2): 1–21.

Lagoudas, D. C. 2008. *Shape Memory Alloys: Modeling and Engineering Applications*. Boston: Springer.

Leo, D. J. 2007. *Engineering Analysis of Smart Material Systems*. Hoboken: John Wiley & Sons, Inc.

Lexcellent, C. 2013. *LES ALLIAGES À MÉMOIRE DE FORME, Série Matériaux (MIM) dirigée par André Pineau*. France: Editions Lavoisier/Hermès.

Lobontiu, N. 2007. *Dynamics of Microelectromechanical Systems*, 2007 ed. USA: Springer.

Papet, P. 2012. *Matériaux piézoélectriques*, edition. France: Technique De L'ingénieur.

Qi, Z. 2011. *Récupération de micro-énergie renouvelable par couplage multiphysique des matériaux : applications aux bâtiments*. L'Université de Grenoble.

Smith, R. 2005. *Smart Material Systems Model Development*. The Society of Industrial and Applied Mathematics.

Stoyanov, L. 2011. "Study of Different Hybrid Systems." Doctoral. thesis, Pascal Paoli University.

Tchawou, E. B., and P. Woafo. 2014. "Harvesting Energy Using a Magnetic Mass and a Sliding Behaviour." *Nonlinear Engineering* 3 (2): 89–97.

"The Alloy That Remembers." 1968. *Time* (Sep 13).

Wang, F. E., W. J. Buehler, and S. J. Pickart. 1965. "Crystal Structure and a Unique Martensitic Transition of TiNi." *Journal of Applied Physics* 36 (10): 3232–9.

Zenati, A. 2007. "Modélisation et simulation de microsystèmes multi domaines à signaux mixtes: vers le prototypage virtuel d'un microsystème autonome." Thèse de Doctorat, L'Université Joseph Fourier.